IEEE Access
Multidisciplinary | Rapid Review | Open Access Journal

Received 16 March 2023, accepted 14 April 2023, date of publication 19 April 2023, date of current version 26 April 2023.

Digital Object Identifier 10.1109/ACCESS.2023.3268521

RESEARCH ARTICLE

Nonlinear Lag Correction Based on the Autoregressive Model for Dynamic Flat-Panel Detectors

EUNAE LEE[1], (Member, IEEE), AND DONG SIK KIM[2], (Senior Member, IEEE)
[1]Advanced Analysis and Data Center, Korea Institute of Science and Technology (KIST), Seoul 02792, South Korea
[2]Department of Electronics Engineering, Hankuk University of Foreign Studies, Yongin 17035, South Korea

Corresponding author: Dong Sik Kim (dskim@hufs.ac.kr)

This work was supported in part by the National Research Foundation of Korea (NRF) grants funded by the Korean Government (MISP) under Grant 2020R1A2C1009895, and in part by the Hankuk University of Foreign Studies Research Fund of 2023.

ABSTRACT Lag signal problems occur in acquiring X-ray image sequences from dynamic flat-panel detectors due to amorphous pixel photodiodes and incomplete readouts. Based on a linear, time-invariant system with a multiple exponential moving average model for the lag signal, Hsieh et al. proposed a recursive deconvolution algorithm for lag corrections, and Starman et al. proposed a nonlinear correction algorithm to cope with nonlinear lag properties. In this paper, we consider an autoregressive model of order 1 to describe lag signals and conduct lag corrections through simple linear and nonlinear decorrelation schemes for the exposure-dependent lag signals. In order to correct the current image frame, using only the previous frame is enough for the autoregressive model. We also evaluate the lag correction performance of the proposed lag correction algorithms by measuring the lag correction factor to show the successful removal of the lag signals with low computational complexities.

INDEX TERMS Autoregressive model, fluoroscopic imaging, lag correction, lag correction factor (LCF), power spectral density (PSD), spectral flatness measure.

NOMENCLATURE

a	Autoregressive coefficient in AR(1).
$a(\mu)$	Exposure-dependent coefficient.
D, R	Difference and the ratio of line mean curves.
f_n, g_n	Signal with lag and independent signal.
g'_n	Decorrelated signal.
g''_n	Recursive deconvolution signal.
q_n	Acquired signal with the electronic noise.
r	Lag correction factor (LCF).
U	Number of pixels per one of an axis.
u_1	Number of pixels per width image.
u^o	X-ray exposure turn-off position in the n=0 frame.
α, ν	Frame gap and the signal per pixel period.
μ	Signal mean.
λ_0, λ_1	Line means of $n = 0$ (X-ray off) and 1.
Φ_f, Φ_g, Φ_ξ	Temporal power spectral density (PSD).
ξ_n, ξ'_n	Electronic noise.
σ_g^2, σ_ξ^2	Variances of g and ξ.

The associate editor coordinating the review of this manuscript and approving it for publication was Qingli Li.

I. INTRODUCTION

Fluoroscopy is a type of medical imaging that shows an X-ray image sequence on a monitor using a direct or indirect dynamic flat-panel detector (FPD) [1]. An indirect dynamic FPD consists of a CsI(Tl)-scintillator layer and photodiodes controlled by an amorphous Si (a-Si) or amorphous InGaZnO (a-IGZO) thin-film transistor (TFT) panel. The charges generated from the X-ray photons are accumulated or stored in the photodiodes and discharged in the scanning step through the TFT array to acquire an image [2]. Here, the accumulated

charges from the previous image frame should be removed from each pixel of the TFT array. However, the lag signal is produced due to the charges trapped in the depletion layer of the amorphous photodiodes [3], [4] and incomplete readouts of the indirect dynamic FPD [5], [6]. The lag signal causes artifacts, such as temporal blurring and image ghosting in the following image frames, and reduces temporal resolutions when an image sequence is acquired [6]. Current dynamic FPDs offer about 1% image mean in the first frame. A certain amount of the lag signal can reduce the noise due to blurring [7]. In this case, using an FPD with no lag and employing digital image processing methods, such as real-time recursive deconvolution [8], can optimize the trade-off between the required temporal resolution and low image noise. Therefore, it is necessary to research and develop a dynamic FPD that generates small lag signals in fluoroscopic imaging.

Hardware approaches also exist to remove the lag signals from an a-Si FPD. The first approach is to insert empty frames at the X-ray source turned off between acquired X-ray frames to remove the lag signal out of the FPD during acquisition [9]. Even though many lag signals can be removed in this way because the lag signal decays exponentially, empty frames increase the image scan time. Furthermore, the charge trapped at deeper energy levels in the band gap will not have emptied and may still contribute to the FPD output. We can use the light-emitting diodes in the second approach to illuminate the TFT panel and saturate the traps between X-ray illumination and FPD readout [10]. With this approach, the lag signal increases in the panel but is made into a uniform offset and causes temporal blurring. Starman et al. [11] investigated a new hardware-based approach to reduce the lag signal in an a-Si FPD based on photodiode biasing and to evaluate its effectiveness at removing shading artifacts in the cone beam computerized tomography reconstructions. They also examined the feasibility of a partially hardware-based solution. However, these methods could not correct the temporal behavior of the scintillator and required hardware redesigns with increased dark currents.

Software approaches can model and correct the lag signals. Most approaches determine a temporal impulse response function (IRF) based on the linear, time-invariant (LTI) moving average (MA) model and then deconvolve it from the raw FPD signal to remove the lag portion from the input signal [3], [12], [13], [14]. Hsieh et al. [3] represented the temporal IRF for afterglows as a multi-exponential signal, where the time constants and coefficients were known a priori for the underlying continuous process [15]. However, when an IRF assumes an LTI system, the measured IRF is highly sensitive to the measurement technique [10]. Furthermore, the residual error still exists in the LTI restorations because of a nonlinearity property that the lag mean portion increases as the exposure decreases [16]. Starman et al. [4] introduced an exposure-dependent lag model and developed the nonlinear consistent stored charge (NLCSC) method to account for the IRF measurement technique and exposure dependencies.

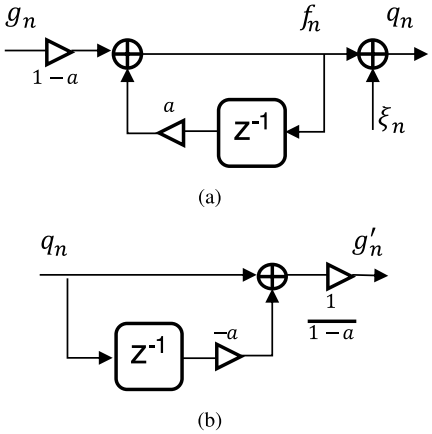

FIGURE 1. AR(1) model for lag signals and the lag correction based on decorrelation signal. (a) AR(1) model with the autoregressive coefficient a and electronic noise ξ_n. (b) Decorrelation step for a lag correction.

Even though NLCSC does not require intimate knowledge of the semiconductor parameters specific to the FPD, the implementation complexity is high to acquire the nonlinear model.

In this paper, we first introduce an autoregressive model of order 1 (AR(1)) to characterize the lag signals instead of the MA model [7], [17]. We next propose linear and nonlinear lag correction algorithms through a simple decorrelation scheme and conduct the lag corrections for X-ray image sequences practically acquired from dynamic FPDs [18]. Lag corrections based on the MA model require iterative deconvolutions in the spatial domain [3]. However, based on the AR(1) model, the proposed algorithm can conduct the lag correction by estimating the autoregressive coefficient and using only the previous frame, which can be conveniently implemented at the field-programmable gate array (FPGA) level. Furthermore, the nonlinear property can be managed using an exposure-dependent autoregressive coefficient. To evaluate the lag correction performance of the developed dynamic FPD, measuring the magnitude of the lag signal is important. We assess its correction performance by measuring the *lag correction factor* (LCF) [5]. Here, we consider low-lag dynamic FPDs with relatively low lag signals in the first frame as small as below 5%, corresponding to an LCF of 0.9.

This paper is organized in the following way. In Section II, we introduce the lag signals based on the AR(1) lag model and propose techniques for measuring the model parameters based on mean and correlation, respectively. We then propose linear and nonlinear decorrelation algorithms in Section III. Performance evaluations of the lag correction algorithms are conducted in Section IV. Simulations and experimental results using X-ray images acquired from dynamic FPDs are shown in Section V. The paper is concluded in the last section.

II. LAG AUTOREGRESSIVE MODEL

In this section, we introduce an AR(1) model for the lag signals in dynamic FPDs. For the AR(1) lag signals, we consider various techniques to estimate the *autoregressive coefficients*.

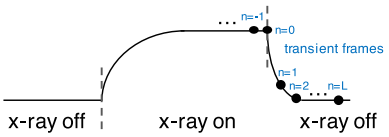

FIGURE 2. Image mean curves with respect to the image frame.

A. AUTOREGRESSIVE MODEL FOR THE LAG SIGNALS

We consider an AR(1) model for lag signals of dynamic FPDs with an autoregressive coefficient a ($0 \leq a < 1$) [17, p. 62]. Letting U be the number of pixels on each axis, a discrete pixel position $\boldsymbol{u}$ can be denoted as $\boldsymbol{u} := (u_1, u_2) \in \{0, \cdots, U-1\}^2$. The resultant image f_n with the lag signal can be defined as an AR(1) stationary sequence:

$$f_n[\boldsymbol{u}] := af_{n-1}[\boldsymbol{u}] + (1-a)g_n[\boldsymbol{u}], \tag{1}$$

where g_n denotes an independent, identically distributed signal from the photon noise of X-rays. We assume that g_n has a Poisson distribution with mean μ [19]. In (1), af_{n-1} implies the lag signal from the previous image frame f_{n-1}. If we consider the electronic noise ξ_n, then the acquired image q_n can be defined as

$$q_n[\boldsymbol{u}] := f_n[\boldsymbol{u}] + \xi_n[\boldsymbol{u}], \tag{2}$$

where ξ_n is an independent, identically distributed signal with mean zero and variance σ_ξ^2 as shown in Fig. 1(a).

B. MEAN-BASED ESTIMATION

In Fig. 2, due to the trapped charges and incomplete readouts from the amorphous photodiodes, the image mean is not zero even after the X-ray is turned off [20]. The autoregressive coefficient a in (1) can be estimated from a ratio of the block image mean of q_n [7], [21] using a transient decaying image sequence of Fig. 2. Here, a can be estimated by

$$a = \frac{E\{q_1\}}{E\{q_0\}}, \tag{3}$$

where $E\{q_0\}$ and $E\{q_1\}$ are acquired at fully X-ray exposed and turn-off conditions, respectively. In (3), the effluence of the electronic noise ξ_n can be ignored because of its zero mean. Note that a pulsed X-ray source should be used with the pulsed fluoroscopy mode in the dynamic FPD to use the relationship of (3) [16], [22], [23].

In an FPD, an X-ray image is acquired from reading out the signal of data lines u_1 while scanning the gate line u_2. If we use a continuous X-ray source with the continuous fluoroscopy mode, then due to the scanning process of reading charges [24], the line-mean curve, denoted as $\lambda_0(u_1)$ and $\lambda_1(u_1)$, obtained along the data-line direction of u_2, shows a linearly decreasing shape after a gate-line position of $u_1 = u^o$, where the X-ray turns off, as shown in Fig. 3. Hence, special consideration is required to obtain a similar to the line mean [24], [25]. For a continuous fluoroscopy mode under an X-ray tube with a constant potential generator [26], a pixel

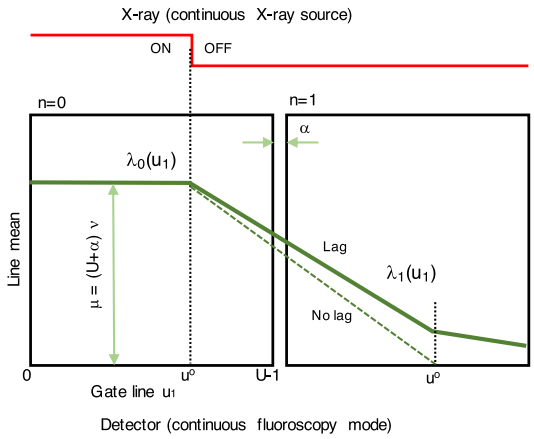

FIGURE 3. Decaying line means, λ_0 and λ_1, of two transient image frames when the X-ray tube turns off at $u = u^o$ of $n = 0$ and 1 in a dynamic FPD.

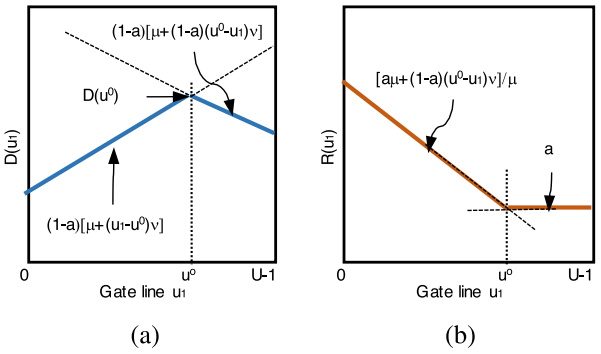

FIGURE 4. Estimations of the autoregressive coefficients a based on the line mean for the AR(1) model. (a) Line mean difference method in (5). (b) Line mean ratio method in (7).

integrates charges during the image frame period of $U + \alpha$ pixels, where α represents the frame gap. Hence, for a given pixel, the signal mean μ can be represented as $\mu := (U+\alpha)\nu$ (DV, digital value), where ν (DV/pixel) is a value yielded for a pixel period and is dependent on the incident exposure [24].

Let $D(u_1)$ denote a difference between the line mean curves of $n = 0$ and $n = 1$, for a scan-line position u_1, and be defined as

$$D(u_1) := \lambda_0(u_1) - \lambda_1(u_1). \tag{4}$$

The difference D can be described with two linear polynomials as shown in Fig. 4(a). The left and right polynomial curves intersect at $u_1 = u^o$ [25, AR3]. Hence, a can be obtained from

$$a = 1 - \frac{D(u^o)}{\mu}. \tag{5}$$

From (5), we can obtain the autoregressive coefficient a using the current image after the X-ray turns off and the previous image.

For narrow X-ray images from fast dynamic detectors, it is hard to find the intersection point u^o. Hence, estimating a from (5) is not easy. Instead of using the difference of (4), we can use a ratio of the line mean curves as follows. Let

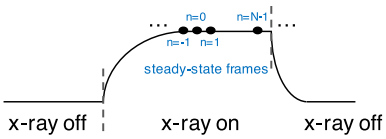

FIGURE 5. Correlation-based methods [5], [7] and the PSD-based method [27] use the steady-state image sequences to measure LCF values.

$R(u_1)$ denote the ratio of the line mean curves of $n = 0$ and $n = 1$, and be defined as

$$R(u_1) := \frac{\lambda_1(u_1)}{\lambda_0(u_1)}. \tag{6}$$

Note that the ratio satisfies the following relationship:

$$a = R(u_1), \tag{7}$$

for $u_1 > u^o$ as shown in Fig. 4(b) [25, AR4]. Even though the ratio R can yield an estimate of a without searching the intersection u^o, the approach based on the ratio R shows unstable or low-precision estimate values, especially at low doses. Hence, using the different approach from (5) is preferable for a wide range of incident exposures.

C. CORRELATION-BASED ESTIMATION

The correlations of f_n can be used to estimate the autoregressive coefficient a [5], [7] using a steady-state image sequence, as shown in Fig. 5. In other words, a can also be estimated by

$$a = \frac{\mathrm{Cov}\{f_n, f_{n+1}\}}{\mathrm{Var}\{f_n\}} = \frac{\mathrm{Cov}\{q_n, q_{n+1}\} - \mathrm{Cov}\{\xi_n, \xi_{n+1}\}}{\mathrm{Var}\{q_n\} - \sigma_\xi^2}. \tag{8}$$

Here, the variance of the electronic noise, σ_ξ^2, can be estimated from dark images, which are acquired without exposure, and can be extracted. Because the lag signal implies the remaining signal mean at the consequent image frames, using the mean-based method of (5) or (7) in estimating the autoregressive coefficient a can provide more accurate results than the correlation-based indirect method of (8) [24].

III. LAG CORRECTION BASED ON THE AUTOREGRESSIVE MODEL

In this section, we propose lag correction algorithms based on the AR(1) model.

We first correct the lag signals from the acquired X-ray images of q_n. Using q_n, the proposed linear lag correction algorithm restores g_n from a *decorrelation scheme* [17, p. 253]:

$$g'_n[\boldsymbol{u}] := \frac{q_n[\boldsymbol{u}] - a q_{n-1}[\boldsymbol{u}]}{1-a}, \tag{9}$$

for each pixel $\boldsymbol{u}$ as shown in Fig. 1(b). Note that (9) is a linear predictive coder [17] and requires only the previous image frame to decorrelate or correct the current image. The estimate g'_n of (9) can be rewritten as

$$g'_n[\boldsymbol{u}] = g_n[\boldsymbol{u}] + \xi'_n[\boldsymbol{u}], \tag{10}$$

where $\xi'_n[\boldsymbol{u}] := (\xi_n - a\xi_{n-1})/(1-a)$ is generated from the electronic noise. Note that the mean of ξ'_n is zero, and the variance is given as

$$\mathrm{Var}\{\xi'_n\} = \frac{1+a^2}{(1-a)^2}\sigma_\xi^2. \tag{11}$$

Because the electronic noise in g'_n satisfies

$$\sigma_\xi^2 \le \mathrm{Var}\{\xi'_n\} \le \left(\frac{1+a}{1-a}\right)^2 \sigma_\xi^2, \tag{12}$$

the restored image g'_n can contain more significant electronic noise levels than the case of q_n [28].

The linear lag correction scheme of (9) can be easily implemented with low computational complexity. For practical dynamic FPDs, however, the autoregressive coefficient of the AR(1) model depends on the signal mean or the incident exposure. Hence, we next introduce a nonlinear lag correction algorithm. The AR(1) model of (1) can be extended to an exposure-dependent nonlinear lag model as

$$f_n[\boldsymbol{u}] = a(f_{n-1}[\boldsymbol{u}])f_{n-1}[\boldsymbol{u}] + [1 - a(f_{n-1}[\boldsymbol{u}])]\, g_n[\boldsymbol{u}], \tag{13}$$

where the exposure-dependent autoregressive coefficient $a(\mu)$ is dependent on the previous signal f_{n-1} changes according to the exposure. The proposed linear lag correction algorithm of (9) can be modified as a nonlinear lag correction algorithm:

$$\frac{q_n[\boldsymbol{u}] - a\,(q_{n-1}[\boldsymbol{u}])\, q_{n-1}[\boldsymbol{u}]}{1 - a\,(q_{n-1}[\boldsymbol{u}])}, \tag{14}$$

for each pixel of $\boldsymbol{u}$. Because the previous signal f_{n-1} is not available from the acquired image sequence, q_{n-1}, which includes the electronic noise ξ_{n-1}, is employed to obtain the correlation coefficient $a(\mu)$ for each pixel of $\boldsymbol{u}$.

IV. PERFORMANCE EVALUATION OF THE LAG CORRECTION

In this section, the performances of the proposed lag correction algorithms are evaluated based on observing the LCF values. Here, an LCF value of 1 implies there are no lag signals. Lee and Kim [25] proposed and summarized several LCF measurement methods based on the MA(L) [25, MA1-MA5] and AR(1) models [25, AR1−AR5].

A. LAG CORRECTION FACTORS BASED ON MEAN

The first-moment methods for measuring LCF use the signal mean of transient decaying image frames acquired from the continuous or pulsed X-ray source [24], [25]. We observe the lag correction performance based on signal means from the LCF measurement methods. The LCF of the lag-corrected signal g'_n of (9) is investigated based on signal means as follows. If the X-ray is tuned off from $n = 1$ as shown in Fig. 2, then $g_n = 0$, for $n \ge 1$, and thus $g'_n = \xi_n$, for $n \ge 1$. Therefore, we can have a mean ratio of $E\{g'_1\}/E\{g'_0\} = 0$ as an estimate of a' from (3). Let r denote the lag correction factor. Because the LCF value for the AR(1) model is given as $r = (1-a')(1+a')$ [25] and $a' = 0$, the LCF value satisfies $r = 1$. Therefore, the corrected signal g'_n has no lags.

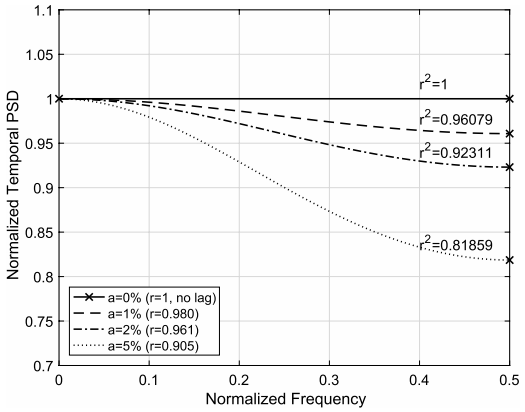

FIGURE 6. Temporal PSD of the AR(1) lag model in (17). The lag system h_n plays a low-pass filter, and thus the PSD curve decreases as the normalized frequency increases to $\omega/2\pi = 0.5$. Note that the LCF for AR(1) satisfies $r = (1-a)/(1+a)$ for a correlation coefficient of a.

B. LAG CORRECTION FACTORS BASED ON CORRELATIONS

We observe the correlations and temporal PSD curves of acquired image sequences based on the AR(1) lag model to evaluate the lag correction performance of the proposed algorithm. The second-moment methods, which use the correlations, including the temporal PSD, use the steady-state second moments of image frames acquired from continuous and pulsed X-ray sources [5], [25].

We first observe the lag correction performance from the correlation-based LCF measurement from (8). For a steady-state image sequence of Fig. 5, it is clear that the covariance of g'_n and g'_{n+1} is equal to zero. Hence, a' is zero for g'_n, and the LCF value is also one. Therefore, the decorrelated signal g'_n has no lag signals.

We next observe the LCF values from the temporal PSD. The IRF of h_n in the AR(1) model can be a causal system: $h_n = (1-a)a^n$, for $n \geq 0$, and 0 otherwise [5], [17]. The acquired image q_n can then be rewritten as an infinite impulse response system as

$$q_n[\boldsymbol{u}] = \sum_{k=0}^{\infty} h_k g_{n-k}[\boldsymbol{u}] + \xi_n[\boldsymbol{u}]. \tag{15}$$

We can also restore g_n from a recursive deconvolution step:

$$g''_n[\boldsymbol{u}] = \frac{q_n[\boldsymbol{u}] - (1-a)as_n[\boldsymbol{u}]}{1-a}, \tag{16}$$

where $s_n[\boldsymbol{u}] := g''_{n-1}[\boldsymbol{u}] + as_{n-1}[\boldsymbol{u}]$, in a similar manner to [3]. Because $s_n = (f_{n-1} + \xi_{n-1})/(1-a)$, g''_n is identical to g'_n of the decorrelation step (9). Let Φ_q denote the temporal PSD of q_n. From (15), Φ_q is given as

$$\Phi_q(\omega) = \frac{(1-a)^2}{1+a^2-2a\cos(\omega)}\sigma_g^2 + \Phi_\xi(\omega), \tag{17}$$

where ω is a normalized radian frequency and Φ_ξ is the temporal PSD of the electronic noise ξ_n [17, p. 64]. In (17), the spectral flatness measure (SFM) of f_n is $1-a^2$, which is less than 1 due to the lag. The PSD of f_n at $\omega = \pi$ is equal to $r^2\sigma_g^2$ and thus decreases as r decreases while the PSD at $\omega = 0$ is fixed to σ_g^2 as illustrated in Fig. 6.

From (15), the LCF from h_n can be rewritten as $r = \sum_{k=0}^{\infty} h_k^2$. Note that, from Parseval's theorem, the PSD of (17) provides the following LCF relationship:

$$r = \frac{1}{2\pi}\int_{-\pi}^{\pi} \frac{(1-a)^2}{1+a^2-2a\cos(\omega)}d\omega = \frac{1-a}{1+a} \tag{18}$$

similarly to the LCF measurement method based on the temporal PSD [27].

We now obtain the temporal PSD of the decorrelated g'_n, which is denoted as $\Phi_{g'}$ and can be given as

$$\Phi_{g'}(\omega) = \sigma_g^2 + \Phi_{\xi'}(\omega). \tag{19}$$

In (19), the PSD of g_n is a correlation of σ_g^2, and thus the LCF value is 1. The second term on the right side of (19) is the PSD of ξ'_n and can be estimated from a dark image sequence. Hence, the PSD curve of the decorrelated g'_n can be flattened or whitened by subtracting $\Phi_{\xi'}$. Therefore, it can be shown that the lag signals are corrected from the proposed algorithm based on the temporal PSD observation.

V. SIMULATION RESULTS

In this section, we conducted simulations and experiments for the lag correction based on the AR(1) model, and dynamic FPDs from DRTECH Co. Ltd. (www.drtech.com) were used. In the dynamic FPDs, the a-IGZO TFT panel with the a-CsI(Tl) scintillator controlled the photodiodes. We measured the autoregressive coefficient a using white images acquired from uniformly exposed X-rays under the RQA5 and Mo/Rh conditions depending on applications [27], [29] and dark images without exposures. We used image mean from a transient decaying image sequence after the X-ray tube tunes off for the line-mean method of (5) or (7). Here, we also used a temporal correlation coefficient from a steady-state image sequence as shown in (8) [5], [7]. The frame rates of the image sequences were 10-30 frames per second (fps).

A. TEMPORAL BLURRING FROM THE LAG SIGNALS

We first observe a synthetic example of temporal blurring due to the lag signal in mammography imaging. Fig. 7(a) shows a processed and enhanced mammography image from RConsole2 (www.drtech.com) and Fig. 7(b) shows a nonlinear lag signal of $a(f_{n-1})f_{n-1}$.

The blurring amount can be observed by measuring MTF degradation for moving object image frames based on parametric MTF modeling and image synthesizing. We first conduct parametric modeling for the FPD MTF [30], [31]. To measure the MTF of a given FPD, we acquire slant-edge images under an appropriate exposure from a slant-edge phantom with a slant-edge angle of $\approx 2.7°$ as described in the IEC62220 standard [27]. We then conduct parametric modeling for the measured FPD MTF [30], [31]. Here, a 3rd-order polynomial fitting is performed on the log value of MTF. Based on synthesized moving edge images under the

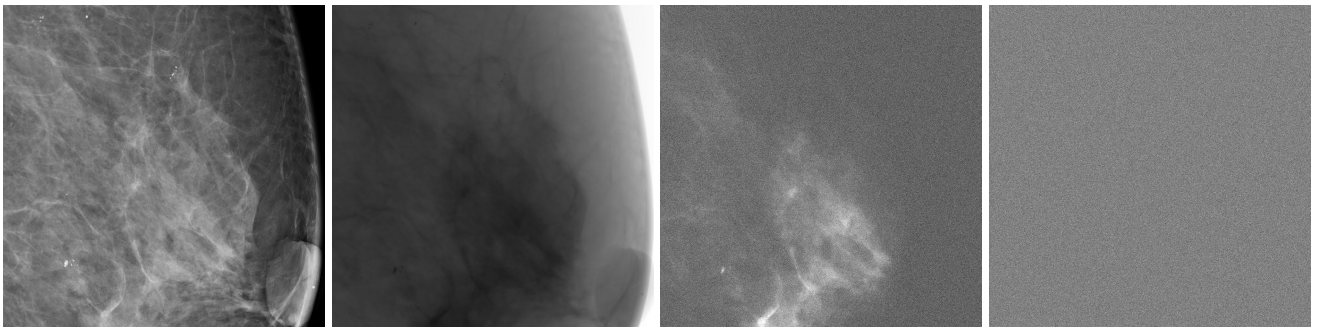

FIGURE 7. Synthetic examples to show nonlinear lag corrections. (a) Mammography image from RConsole2 (DRTECH, Co.Ltd., www.drtech.co.kr). (b) Lag signal of $a(f_{n-1})f_{n-1}$. (c) After the linear lag corrections of (9), the lag signal remains with breast calcifications. (d) After the nonlinear lag correction of (14), the lag signals are removed.

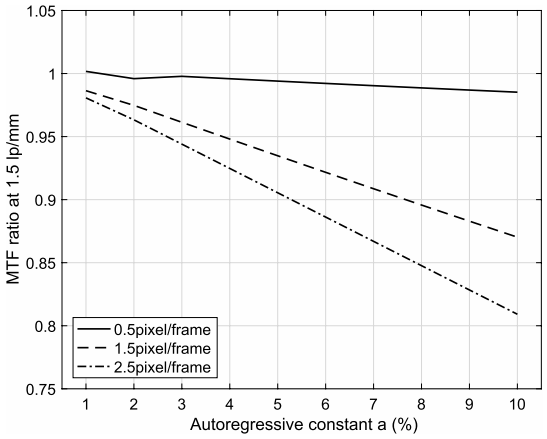

FIGURE 8. Simulation of the MTF degradation from the lag signal for different values of the autoregressive coefficient a in percentage. The MTF degradation is calculated for the MTF value of 0.489 at 1.5 lp/mm, where the pixel pitch is 140 μm/pixel.

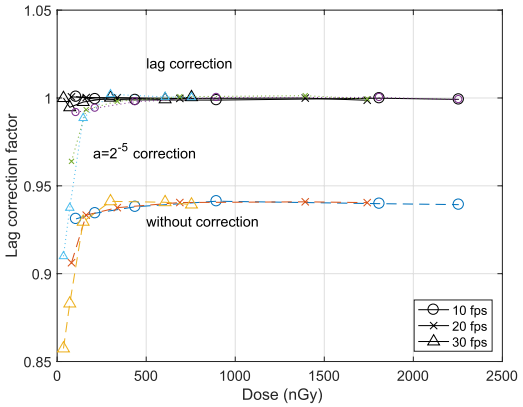

FIGURE 9. Lag corrections of (9) and (14), and the LCF values measured from the mean-based method of Kim and Lee [24, Algorithm 1], [25, MA4] using transient decaying image sequences of Fig. 2 under RAQ5 [27]. The obtained correlation coefficients are shown in Fig. 10. The correction results are also shown with a fixed $a = 2^{-5}$ (3.25%).

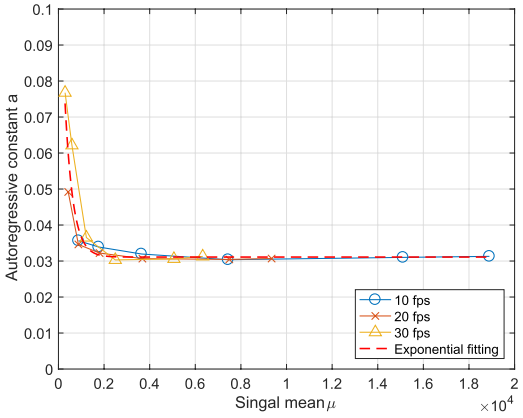

FIGURE 10. Fitting for $a(\mu)$ to cope with high lag signals at low doses. A fitting curve is given as $a(\mu) \approx \alpha e^{-\mu/\tau} + \beta$, where $\alpha = 0.0980$, $\beta = 0.0311$, and $\tau = 350$.

AR(1) lag model of (1), we observe MTF degradations as shown in Fig. 8. Even for a slight lag of $a = 1\%$, movements of 1.5 and 2.5 pixels per frame show MTF degradations of 1.4% and 2.0%, respectively. Besides these temporal blurring artifacts, a lag signal of $a = 1\%$ also shows a ghost image artifact.

B. LAG CORRECTION SIMULATION RESULTS

Using practically acquired X-ray image sequences, we next validate the lag correction performance through the LCF values measured from the mean-based method [24, Algorithm 1] for transient decaying image sequences. The acquired images show lag signals from the measured LCF values as "without correction" in Fig. 9. Note that the LCF values decrease significantly at low doses independently of the frame rates [24], [25]. If we apply the nonlinear lag correction of (14), then the corrected images show the LCF values increased to ≈ 1.0 for the whole dose range as "lag correction." Here, the exposure-dependent autoregressive coefficient $a(\mu)$ was obtained by a curve fitting as shown in Fig. 10.

In Fig 9, lag correction results with a fixed coefficient of $2^{-5} = 0.0325$ in (9) are also depicted as "$a = 2^{-5}$ correction." This value is close to 0.0311, obtained at relatively high doses, as shown in Fig. 10. Note that multiplying 2^{-5} to the previous frame f_{n-1} can be efficiently conducted by 5-bits

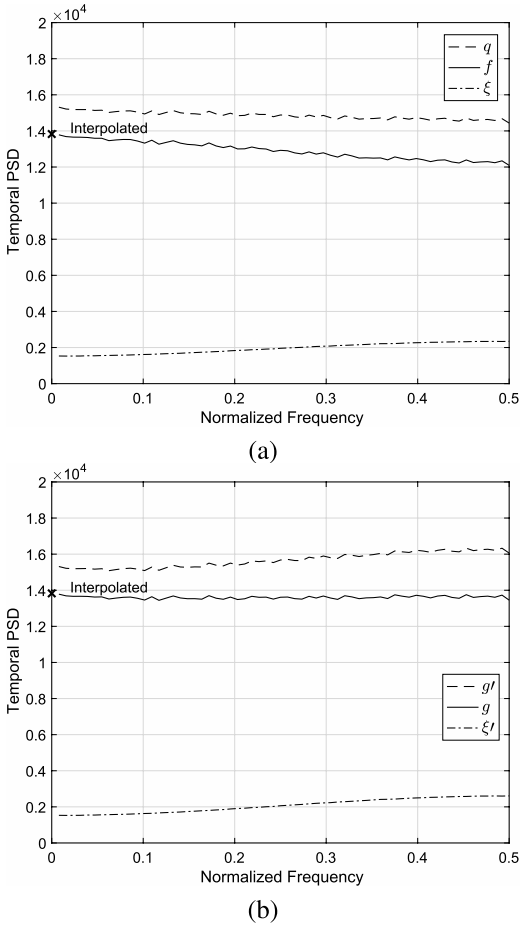

FIGURE 11. Comparison of the temporal PSD curves with respect to ω/π for an image sequence acquired at an incident dose of 1,393 nGy with a frame rate of 20 fps (the PSD size was $N = 128$). (a) Temporal PSD curves of g, f, and ξ. The LCF and SFM values are 0.949 and 0.999, respectively ($\sigma = 2.61\%$). (b) Temporal PSD curves of the lag correction from the linear decorrelation step of (9). The LCF and SFM values are 1.00 ($\sigma = 0\%$).

shifting binary values in (9). Hence, the lag correction of (9) can be easily implemented with low computational complexities. However, the lag correction performance is not good at relatively low doses, as observed in Fig. 7(c). The breast calcifications with low pixel values can remain as lag signals if the linear lag correction of (9) is applied. On the other hand, if the nonlinear lag correction of (14) is used, then the lag signal of low doses can be efficiently removed, as shown in Fig. 7(d). Note that the electronic noise in Fig. 7(d) depends on the lag signal. However, the lag dependency is invisible; thus, the nonlinear lag correction algorithm can successfully correct the nonlinear lag signals.

C. PSD AND CORRELATION SIMULATION RESULTS

In Fig. 11, we illustrate an example of temporal PSD curves to show the decorrelation step of (9) and SFM values. Here, to alleviate the nonuniform temporal gain problem for the approaches of PSD and correlations, we use a correction scheme called the upper-lower algorithm based on a notion of image difference [5], [32], [33].

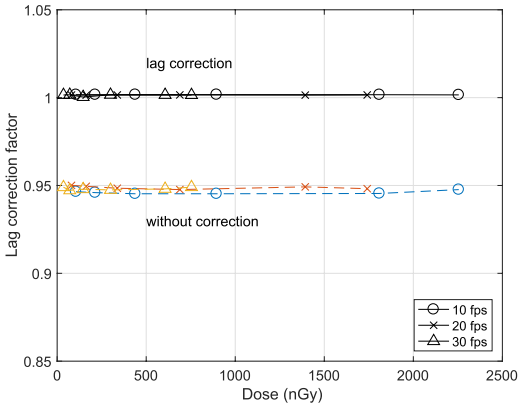

FIGURE 12. Lag correction of (9) and the LCF values measured from the correlation-based method of Matsunaga et al. [5], [7] using steady-state image sequences of Fig. 5 under RQA5 [27].

The PSD of f_n ("f") was obtained by subtracting the PSD of the electronic noise ξ_n ("ξ") from the PSD of the acquired image q_n ("q"). We can observe in Fig. 11(a) that the PSD of f_n decreases as the frequency increases, as shown in (17). After decorrelating the lag signals, we observe a flat spectrum in Fig. 11(b) with an SFM value of ≈ 1 ("g") as shown in (19). We can observe that the PSD values of the electronic noise, ξ_n, and ξ'_n, slightly increase as the frequency increases (11ξ" and 11ξ'") [24], [25].

We now observe a comparison result of the lag correction for several incidents doses in Fig. 12. Here, the LCF values of the corrected image sequences are measured based on the correlation-based method of Matsunaga et al. [7] for steady-state image sequences of Fig 5. For the measuring method of Matsunaga et al., we observe that the average LCF value increased to 1.002 from 0.946 by conducting the lag correction of (9). On the other hand, the correlation-based method does not show such decreasing LCF values as the dose decreases. Hence, the LCF values show different properties according to the mean-based or correlation-based measurement methods. Because the lag artifacts are generally caused by the lag signal mean, the decreasing LCF values in Fig 9 imply that the lag property is worsening, especially at low doses. Hence, the autoregression coefficient measured by a mean-based method in Fig. 9 can provide further accurate lag correction performances.

VI. CONCLUSION

In this paper, we considered an AR(1) model to describe lag signals and conducted lag corrections through a decorrelation step for X-ray image sequences practically acquired from dynamic FPDs. Due to the simple step from the AR(1) model, we could conduct lag corrections by using only the previous image frame with low computational complexities. The lag correction performance was also evaluated through LCF and showed successful removal of the lag signals. The linear lag correction with a fixed autoregressive coefficient 2^{-5} could implement a simple lag correction with the FPGA level. The nonlinear lag correction algorithm could

correct the exposure-dependent lag signals by introducing an exposure-dependent autoregressive coefficient of AR(1).

REFERENCES

[1] J. T. Bushberg, J. A. Seibert, J. E. M. Leidholdt, and J. M. Boone, *The Enssential Physics of Medical Imaging*, 2nd. ed. Philadelphia, PA, USA: Lippincott Williams & Wilkins, 2002.

[2] J. A. Rowlands and J. Yorkston, "Flat panel detectors for digital radiography," in *Handbook of Medical Imaging*, vol. 1. Washington, DC, USA: SPIE, 2000, ch. 4.

[3] J. Hsieh, O. E. Gurmen, and K. F. King, "Recursive correction algorithm for detector decay characteristics in CT," *Proc. SPIE*, vol. 3977, pp. 298–305, Apr. 2000.

[4] J. Starman, J. Star-Lack, G. Virshup, E. Shapiro, and R. Fahrig, "A nonlinear lag correction algorithm for a-Si flat-panel X-ray detectors," *Med. Phys.*, vol. 39, no. 10, pp. 6035–6047, 2012.

[5] D. S. Kim and E. Lee, "Signal lag measurements based on temporal correlations," *IEEE Signal Process. Lett.*, vol. 28, pp. 21–25, 2021.

[6] E. Lee and D. S. Kim, "Correlation-based lag correction factor measurements for flat-panel dynamic detectors," *J. Inst. Electron. Inf. Eng.*, vol. 59, no. 4, pp. 71–78, 2022.

[7] Y. Matsunaga, F. Hatori, H. Tango, and O. Yoshida, "Analysis of signal to noise ratio of photoconductive layered solid-state imaging device," *IEEE Trans. Electron Devices*, vol. 42, no. 1, pp. 38–42, Jan. 1995.

[8] C. Dydula, G. Belev, and P. C. Johns, "Development and assessment of a multi-beam continuous-phantom-motion X-ray scatter projection imaging system," *Rev. Sci. Instrum.*, vol. 90, no. 3, 2019, Art. no. 035104.

[9] J. Siewerdsen and D. Jaffray, "Cone-beam computed tomography with a flat-panel imager: Effects of image lag," *Med. Phys.*, vol. 26, no. 12, pp. 2635–2647, 1999.

[10] J. Starman, J. Star-Lack, G. Virshup, E. Shapiro, and R. Fahrig, "Investigation into the optimal linear time-invariant lag correction for radar artifact removal," *Med. Phys.*, vol. 38, no. 5, pp. 2398–2411, 2011.

[11] J. Starman, C. Tognina, L. Partain, and R. Fahrig, "A forward bias method for lag correction of an a-Si flat panel detector," *Med. Phys.*, vol. 39, no. 1, pp. 18–27, 2012.

[12] H. C. Andrews and B. R. Hunt, *Digital Image Restoration*. New Jersey, NY, USA: Prentice-Hall, 1977.

[13] R. L. Weisfield, M. A. Hartney, R. Schneider, K. Aflatooni, and R. Lujan, "High-performance amorphous silicon image sensor for X-ray diagnostic medical imaging applications," in *Proc. SPIE*, vol. 3659, pp. 307–317, May 1999.

[14] N. Mail, D. J. Moseley, J. H. Siewerdsen, and D. A. Jaffray, "An empirical method for lag correction in cone-beam CT," *Med. Phys.*, vol. 35, no. 11, pp. 5187–5196, 2008.

[15] A. Avakyan, I. Dergacheva, A. Elanchik, T. Krylova, T. Lobzhanidze, S. Polikhov, and V. Smirnov, "Investigation of the lag effect in X-ray flat-panel detector for cone-beam computed tomography," *Biomed. Eng.*, vol. 54, no. 3, pp. 179–183, 2020.

[16] J. T. Bushberg, J. A. Seibert, J. E. M. Leidholdt, and J. M. Boone, *The Essential Physics of Medical Imaging*, 4th ed. New York, NY, USA: Wolters Kluwer, 2021.

[17] N. S. Jaynat and P. Noll, *Digital Coding of Waveforms: Principles and Applications to Speech and Video*. Upper Saddle River, NJ, USA: Prentice-Hall, 1984.

[18] E. Lee and D. S. Kim, "Lag signal modeling based on an autoregressive model and lag corrections," in *Proc. IEEE NSS/MIC/RTSD*, Milano, Italy, 2022, pp. 1–2.

[19] A. Macovski, *Medical Imaging Systems*. Upper Saddle River, NJ, USA: Prentice-Hall, 1983.

[20] Q. Wu, Z. Ling, C. Zhang, Q. Zhou, X. Wang, W. Yuan, and S.-N. Zhang, "Investigating the image lag of a scientific CMOS sensor in X-ray detection," *Nucl. Instrum. Methods Phys. Res. Sect. A, Accel., Spectrometers, Detect. Associated Equip.*, vol. 1050, May 2023, Art. no. 168180.

[21] P. R. Granfors and R. Aufrichtig, "DQE(f) of an amorphous-silicon flat-panel X-ray detector: Detector parameter influences and measurement methodology," in *Proc. SPIE*, vol. 3977, pp. 2–13, Apr. 2000.

[22] R. J. Wilks, *Principles of Radiological Physics*, 2nd. ed. Edinburgh, Scotland: Churchill Livingston, 1987.

[23] J. M. Boone, *X-Ray Production, Interaction, and Detection in Diagnostic Imaging*, vol. 1. Washington, DC, USA: SPIE, 2000, ch. 1.

[24] D. S. Kim and E. Lee, "Measurement of the lag correction factor in low-dose fluoroscopic imaging," *IEEE Trans. Med. Imag.*, vol. 40, no. 6, pp. 1661–1672, Jun. 2021.

[25] E. Lee and D. S. Kim, "Linear lag models and measurements of the lag correction factors," *IEEE Access*, vol. 10, pp. 49101–49113, 2022.

[26] R. Aufrichtig, P. Xue, C. W. Thomas, G. C. Gilmore, and D. L. Wilson, "Perceptual comparison of pulsed and continuous fluoroscopy," *Med. Phys.*, vol. 21, no. 2, pp. 245–256, 1994.

[27] *Medical Electrical Equipment Characteristics of Digital X-Ray Imaging Devices—Part1-3: Determination of the Detective Quantum Efficiency Detectors Used in Dynamic Imaging*, document IEC 62220-1-3, Geneva, Switzerland, 2007.

[28] E. Lee and D. S. Kim, "Noise effect on the lag correction for the CsI(Tl)-scintillator flat-panel detectors," in *Proc. 32th Int. Tech. Conf. Circuits/Syst., Comput. Commun. (ITC-CSCC)*, 2017, pp. 939–941.

[29] *Medical Electrical Equipment Characteristics of Digital X-Ray Imaging Devices—Part1-2: Determination of the Detective Quantum Efficiency Detectors Used in Mammography*, document IEC 62220-1-2, Geneva, Switzerland, 2007.

[30] D. S. Kim, "Parametric modeling for indirect flat-panel detectors in radiography imaging," in *Proc. 37th Int. Tech. Conf. Circuits/Syst., Comput. Commun. (ITC-CSCC)*, 2022, pp. 202–204.

[31] D. S. Kim, "Convex combination of images from dual-layer detectors for high detective quantum efficiencies," *IEEE Trans. Biomed. Eng.*, early access, Dec. 14, 2022, doi: 10.1109/TBME.2022.3228892.

[32] D. S. Kim, "Noise power spectrum measurements in digital imaging with gain nonuniformity correction," *IEEE Trans. Image Process.*, vol. 25, no. 8, pp. 3712–3722, Aug. 2016.

[33] D. S. Kim and E. Lee, "Empirical noise power spectrum based on the image subtraction in radiography imaging," in *Proc. IEEE NSS/MIC/RTSD*, Strasbourg, France, 2016, pp. 1–4.

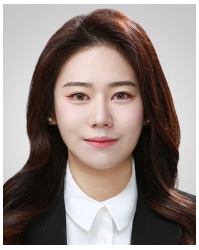

EUNAE LEE (Member, IEEE) received the B.S., M.S., and Ph.D. degrees from the Hankuk University of Foreign Studies, South Korea, in 2014, 2017, and 2022, respectively. She is currently a Postdoctoral Researcher with the Advanced Analysis and Data Center, Korea Institute of Science and Technology (KIST), South Korea. Her research interests include biomedical image processing and medical physics based on machine learning and statistical signal processing.

DONG SIK KIM (Senior Member, IEEE) received the B.S., M.S., and Ph.D. degrees in electrical engineering from Seoul National University, Seoul, South Korea, in 1986, 1988, and 1994, respectively. From 1998 to 1999, he was a Visiting Assistant Professor with the School of Electrical and Computer Engineering, Purdue University, West Lafayette, IN, USA. Since 1986, he has been the Research Director of Automan Company Ltd., South Korea, where he has conducted RF circuit design projects. He is currently a Professor with the Hankuk University of Foreign Studies, South Korea. His research interests include the theory of quantization, biomedical image processing, medical physics, sensor networks, and smart grid based on statistical signal processing. He was a co-recipient of the 2003 International Workshop on Digital Watermarking Best Paper Prize.